Smart Structures and Systems, *Vol. 20, No. 1 (2017) 85-97*
DOI: https://doi.org/10.12989/sss.2017.20.1.085

Semi-active vibration control using experimental model of magnetorheological damper with adaptive F-PID controller

Asan G.A. Muthalif*, Hasanul B. Kasemi, N.H. Diyana Nordin, M.M. Rashid and M. Khusyaie M. Razali

Smart Structures, Systems and Control Research Laboratory (S^3CRL)
Department of Mechatronics Engineering, International Islamic University Malaysia,
Jalan Gombak, 53100, Kuala Lumpur, Malaysia

(Received April 6, 2016, Revised June 9, 2017, Accepted June 14, 2017)

Abstract. The aim of this research is to develop a new method to use magnetorheological (MR) damper for vibration control. It is a new way to achieve the MR damper response without the need to have detailed constant parameters estimations. The methodology adopted in designing the control structure in this work is based on the experimental results. In order to investigate and understand the behaviour of an MR damper, an experiment is first conducted. Force-displacement and force-velocity responses with varying current have been established to model the MR damper. The force for upward and downward motions of the damper piston is found to be increasing with current and velocity. In cyclic motion, which is the combination of upward and downward motions of the piston, the force with hysteresis behaviour is seen to be increasing with current. In addition, the energy dissipated is also found to be linear with current. A proportional-integral-derivative (PID) controller, based on the established characteristics for a quarter car suspension model, has been adapted in this study. A fuzzy rule based PID controller (F-PID) is opted to achieve better response for a varying frequency input. The outcome of this study can be used in the modelling of MR damper and applied to control engineering. Moreover, the identified behaviour can help in further development of the MR damper technology.

Keywords: magnetorheological damper; semi-active vibration; fuzzy-PID; adaptive control

1. Introduction

Magnetorheological (MR) fluid belongs to smart materials due to the ability of controlling its physical properties. MR fluid contains a suspension of 20-30% by volume of relatively pure, soft iron particles immersed in a carrier fluid. It responds to an applied magnetic field with a change in rheological behaviour due to the suspended magnetic particles. In the presence of the applied field, it reversibly changes from free-flowing state (Fig. 1(a)) to a semi-solid state (Fig. 1(b)). This process is due to the iron particles acquiring a dipole moment aligned with the external field which causes the particles to form linear chains parallel to the field, which occurs in the region highlighted in Fig. 2.

This arrangement of the particles solidifies the fluid and thus, restricts the fluid movement. Therefore, a yield strength is developed within the fluid. As the magnetic field increases, the parallel chains become stronger which directly increases the viscosity of the fluid within a very short period of time. These particles can be suspended in water, mineral oil, synthetic oil, or glycol. Additives are also commonly added to discourage gravitational settling and increase the dispersion stability (Hato *et al.* 2011, Piao *et al.* 2014, Quan *et al.* 2013, Song *et al. 2009*).

The initial discovery and development of MR fluids can be credited to Rabinow (1948) of US National Bureau of Standards in the late 1940s. The advantages of MR fluid include high yield stress and high dynamic range; which results in a low power consumption, a small and simple mechanism, non-sensitiveness to impurities, higher range of working temperature (-40 to 150℃) and wider choice of additives (Gordanijed and Kelso 2000, Avraam 2009, Yang *et al.* 2012). These characteristics allow it to be used in vehicle suspensions (Tsampardoukas *et al.* 2008, Kwak *et al.* 2014, Sun *et al.* 2016) , positional and velocity control of pneumatic actuator systems (Huang *et al.* 2002), rehabilitation devices (Dong *et al.* 2006, Nakano and Nakano 2014), prosthetic legs (Kim and Oh 2001, Ekkachai *et al.* 2014, Sayyaadi and Zareh 2015, Diyana Nordin *et al.* 2015), haptic devices (Antolini *et al.* 2013, Nhuyen *et al.* 2013, Najmaei *et al.* 2015, Yin *et al.* 2016), seismic structure control (Caterino *et al.* 2011) and some other interesting areas. MR devices can be easily driven by common low-voltage power sources (Carlson and Jolly 2000). They can also be controlled with a low-voltage, current-driven power supply having only 1~2 amps output which can be provided with batteries.

The operations of MR devices can be classified as operating either in: valve mode, direct shear mode, squeeze mode, or in a combination of these modes, as shown in Fig. 3 (Carlson and Jolly 2000, Wang and Liao 2011). Pressure-driven flow mode (either with fixed poles or with valves)

*Corresponding author, Professor
E-mail: asan@iium.edu.my; asan@cantab.net

ISSN: 1738-1584 (Print), 1738-1991 (Online)

corresponds to Hagen–Poiseuille flow. In this mode, the fluid moves in between the surfaces (through the gap). The magnetic field lines are orthogonal to the flow direction. Devices that operate in this mode include dampers, shock absorbers and valves. In addition, this mode is suitable for car suspension applications as it can provide larger damping force and displacements. On the other hand, direct shear mode, with relatively movable poles, is driven by virtue of attraction forces acting on the fluid between the magnetisable particles. This mode corresponds to Couette flow. Devices operating in this mode include clutches, brakes, locking devices, dampers for small displacements and medium-frequency applications. In addition, in squeeze-film mode, the surface moves in parallel to the magnetic field lines. Devices operating in this mode include dampers which are used in high-force and low-motion applications.

It has been found difficult to get a simple MR damper model because of the significant non-linearity. Researchers have developed numerous models of MR damper earlier; both quasi-static and dynamic models. The quasi-static models successfully describe the force-displacement characteristics of the damper but are unable to explain the non-linearity in force-velocity response. On the other hand, the dynamic models (such as Bingham plastic model, Bouc-Wen model, modified Bouc-Wen model and biviscous) requires a number of parameters to be identified, in order to accurately represent the characteristic of the damper (Zong *et al.* 2013, Cha and Agrawal 2016, Priya and Gopalakrishnan 2016). Thus, employing Lookup table to represent the MR damper seems to be practical in dealing with this issue.

This paper presents experimental study of the dynamic behaviour of MR fluid damper for semi-active vibration control of a quarter car suspension system.

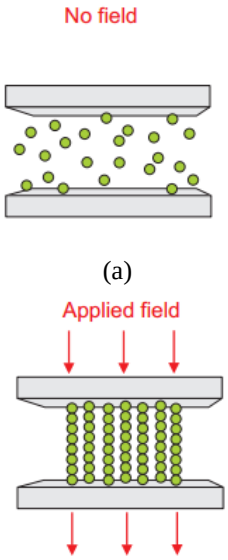

Fig. 1 The arrangement of the particles in MR fluid at (a) no field and (b) with applied field (Avraam 2009)

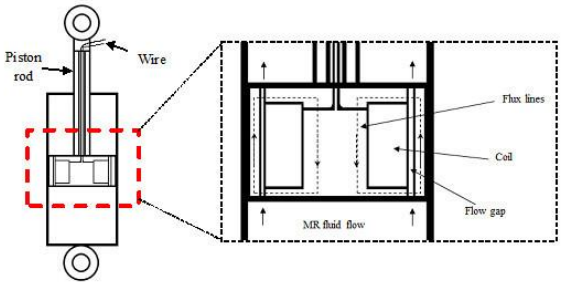

Fig. 2 Schematic of a typical MR damper, focusing on the piston (as shown in the box)

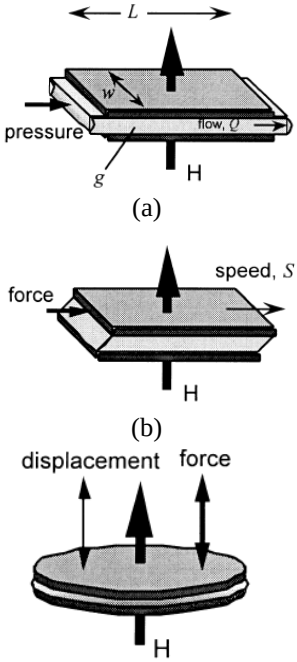

Fig. 3 Operating modes of a magnetorheological fluid damper (a) Pressure-driven flow mode, (b) Direct shear mode and (c) Squeeze-film mode [L=plate length, w=plate width. g=gap size, H = magnetic field] (Carlson and Jolly 2000)

It establishes force displacement behaviour and solves the issues of evaluating too many parameters raised in modelling of MR damper by implementing Lookup table in controller design stage. This study is based on the experimental results and the main contribution is to achieve a new performance based on the model of the MR damper where the experimental analysis and the performance analysis are the key to the methodology. A controller was then simulated using the model of quarter car suspension system and presented with the results. Here, adaptive Fuzzy-PID controller is used as the implementation of Fuzzy controller in semi active system seems to be viable in varying frequency conditions (Makihara *et al.* 2013, Babesse *et al.* 2016). Results of this study may serve to

support in the modelling of MR damper in control applications.

The rest of this paper is organized as follows: Section 2 gives the experimental setup and result analysis; Section 3 discusses controller development; Section 4 concludes the work done in the paper.

2. Experimental setup to establish MR damper characteristics

An MR damper with a total stroke length, L of 74 mm (LORD RD-8041-1 MR damper, shown in Fig. 4(a)) and a maximum current capacity of 2A was investigated in the experiment. During the experiment, the force and the displacement were analysed for different velocities and different initial positions of the stroke. The total stroke length is divided into 4 sections (which are A-B, B-C, C-D and D-E) with an equal length of L/4 mm. Three initial stroke positions were then assigned to test the performance of the damper with respect to the stroke positions. Points B, C and D were defined as the first stroke position, mid stroke position and third stroke position, respectively (Fig. 4). The test setup is shown in Fig. 5.

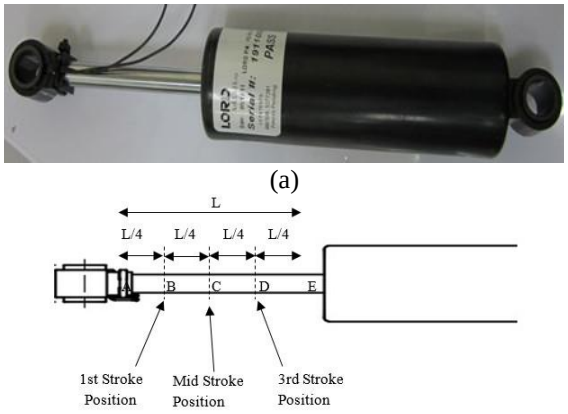

Fig. 4 (a) Actual damper used in the experiment and (b) Different stroke length positions, as marked on the piston rod

Table 1 Typical properties of RD-8041-1 MR damper (courtesy: LORD technical data sheet for RD-8041-1)

Typical Properties		Value
Stroke, mm (in)		74 (2.91)
Extended Length, mm (in)		248 (9.76)
Body Diameter, mm (in)		42.1 (1.66) max
Shaft Diameter, mm (in)		10 (0.39)
Tensile Strength, N (lbf)		8896 (2000) max
Damper Forces, N (lbf) Peak to Peak	5 cm/sec and 1 A	>2447 (>550)
	20 cm/sec and 0 A	<667 (<150)
Operating Temperature, ℃ (℉)		71 (160) max

Table 2 Electrical properties of RD-8041-1 MR damper (courtesy: LORD technical data sheet for RD-8041-1)

Electrical Properties		Value
Input Current, A	Continuous for 30 seconds	1 max
	Intermittent	2 max
Input Voltage, Volt		12 DC
Resistance, ohms	at ambient temperature	5
	at 71℃ (160℉)	7

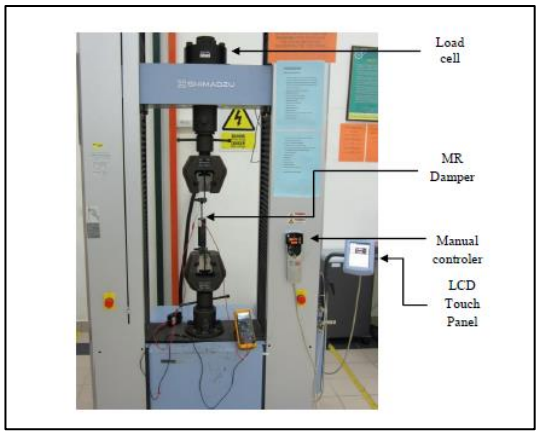

Fig. 5 Universal testing machine used for experimental setup

2.1 Force-displacement characteristics

The response of the damper at three different stroke positions are plotted in Figs. 6 and 7.

The applied current is varied from 0 A to 1 A, with an increment of 0.2 A.

At a small displacement, a visible step function is observed at the damper's force-displacement characteristics. Based on this observation, the responses are further divided into three sections i.e. before the step, during step and after the step (Fig. 6(a)). The first and second sections are common in a way that it will rise before reaching steady state. These are the results of the particle movement having chain-like structures in MR fluid.

In the third section, during the downward motion of the piston (compression), the carrier fluid tends to push itself out of the compressive region. As the displacement increases, the tendency for this phenomenon also increases. However, due to the existence of the particles inside the damper, the expulsion cannot be properly done due to the resistance caused by the particles' density and the inter particles' attraction force. Therefore, in this region, the volume fraction of the particle is assumed to increase as only the carrier fluid is being expelled (Mazlan *et al.* 2007). In general, when the density of the particle increases, more force is needed to cause the fluid to flow. As this happens in a region, the effective volume of the fluid movement reduces. Thus, it results to a higher resistance to flow, which requires more force.

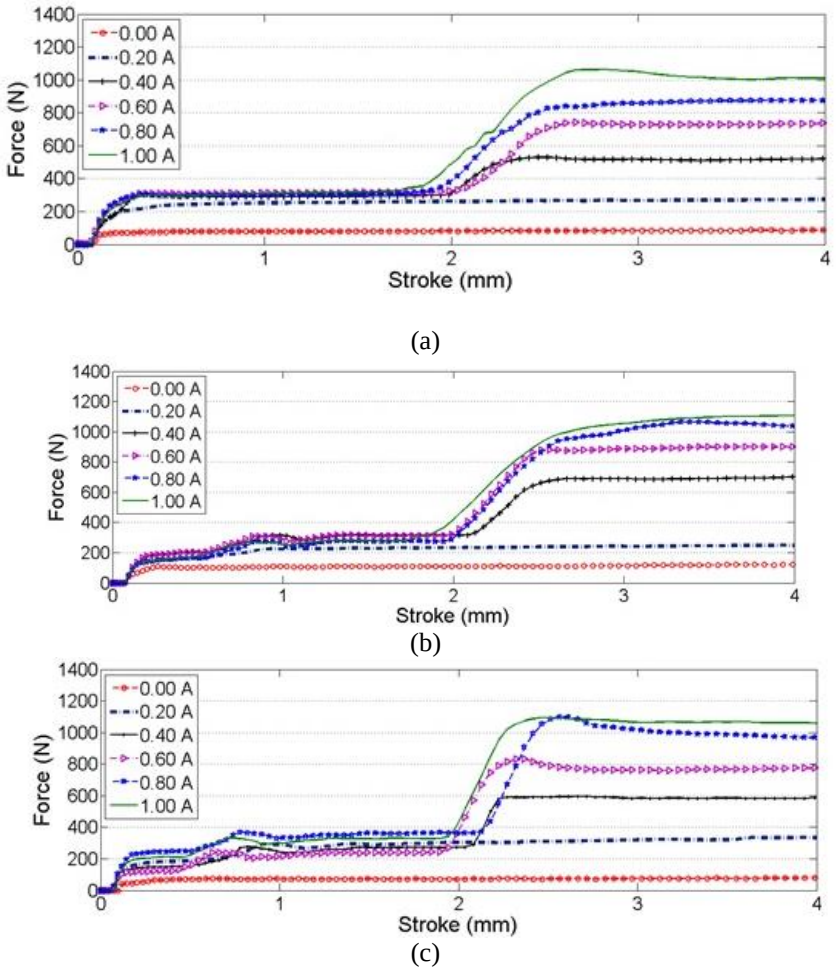

Fig. 6 Experimental results of downward motion at (a) first stroke position, (b) mid stroke position and (c) third stroke position

The amount of force needed to break the chain of a single column made by particles of the same size due to the presence of the magnetic field strength is expected to be the same throughout the MR fluid. Again, if the field current rises, the tendency of forming thicker chain-columns also increases. This is because more particles are attracted to each other to form the chain in the direction of the magnetic field. The force required to yield thicker chains is higher. In upward motion (tensile), this third section is not present due to a lesser amount of particle resistances.

2.2 Force-velocity characteristics

The amount of force generated depends on the stroking velocity as well. Lower piston velocity gives lower force amplitude, while higher velocity gives higher force as shown in Fig. 8. Here, for a particular current, the mechanical energy needed to yield the chain-like structures at a certain velocity is constant. However, at the same value of applied current, if the velocity increases, a higher energy is needed to yield the chain-like structures. Hence, force required to yield the chain structures is higher at a higher velocity and much smaller at a lower velocity region.

2.3 Force, current and displacement characteristics in cyclic motion mode

Fig. 9 shows force-displacement (stroke length) responses for varying currents at three different stroke positions in cyclic motion. Here, the cycle stroke is set to 12 mm and the piston moves at 500 mm/min. These plots show the hysteresis characteristics of the MR damper. Various stroke position results are also compared in Fig. 10.

In Figs. 9 and 10, it is observed that the force at the third stroke position of the cyclic mode response is higher than that of the first and mid stroke positions. It is obvious that during the third stroke, there exists an additional operating mode as the piston moves towards the end. This mode, which is identified as the squeeze mode, tries to expel the carrier fluid out while at the same time, the suspended particles try to resist this expulsion.

The combination of direct shear and squeeze modes results in a higher force at the third stroke position. Therefore, the volume of the response is higher, and thus the amount of energy being dissipated is also larger. The energy dissipated through the cyclic mode is calculated from the area of the hysteresis plot of every individual current.

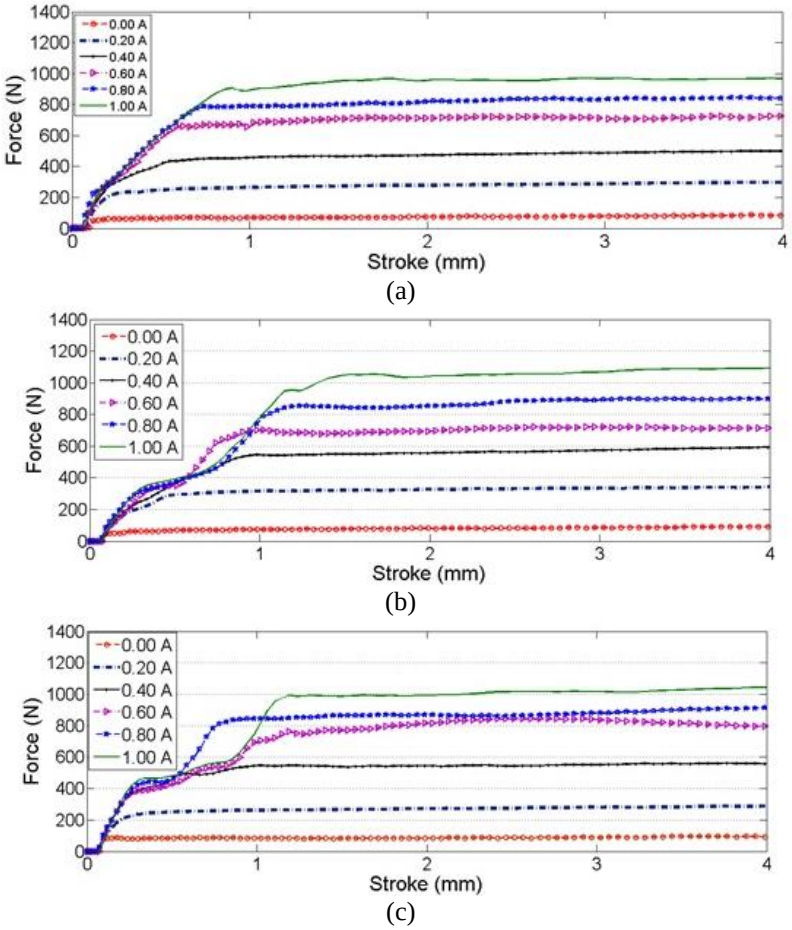

Fig. 7 Experimental results of upward motion at (a) first stroke position, (b) mid stroke position and (c) third stroke position

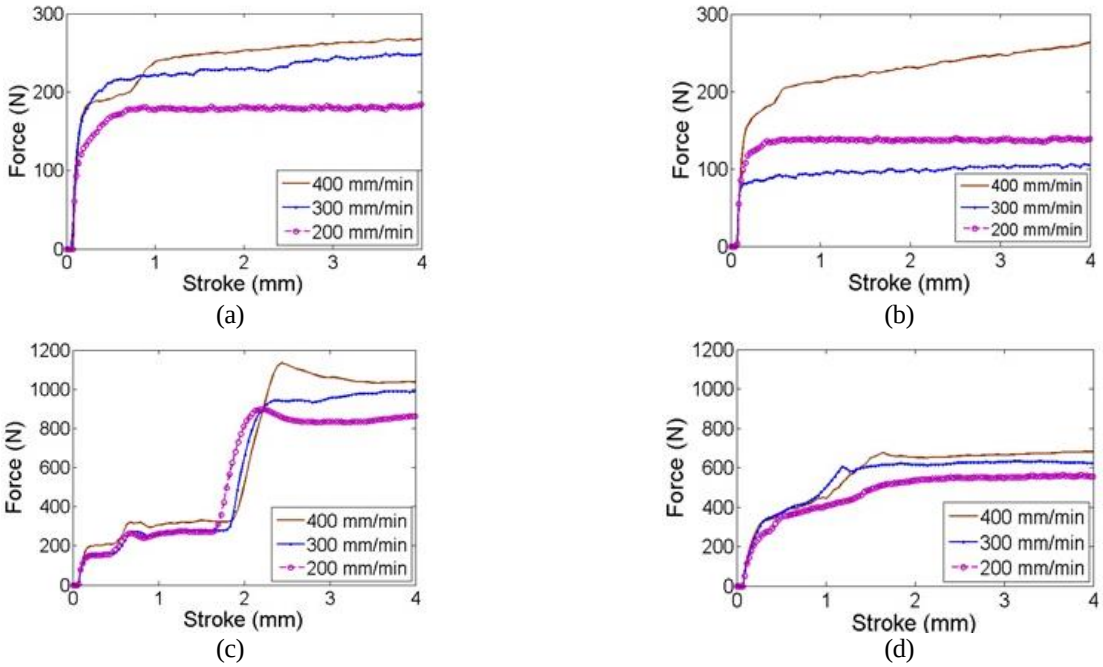

Fig. 8 Experimental results at mid stroke position at various velocities: (a) downward at 0.10 A, (b) upward at 0.10 A, (c) downward at 0.60 A and (d) upward at 0.60 A

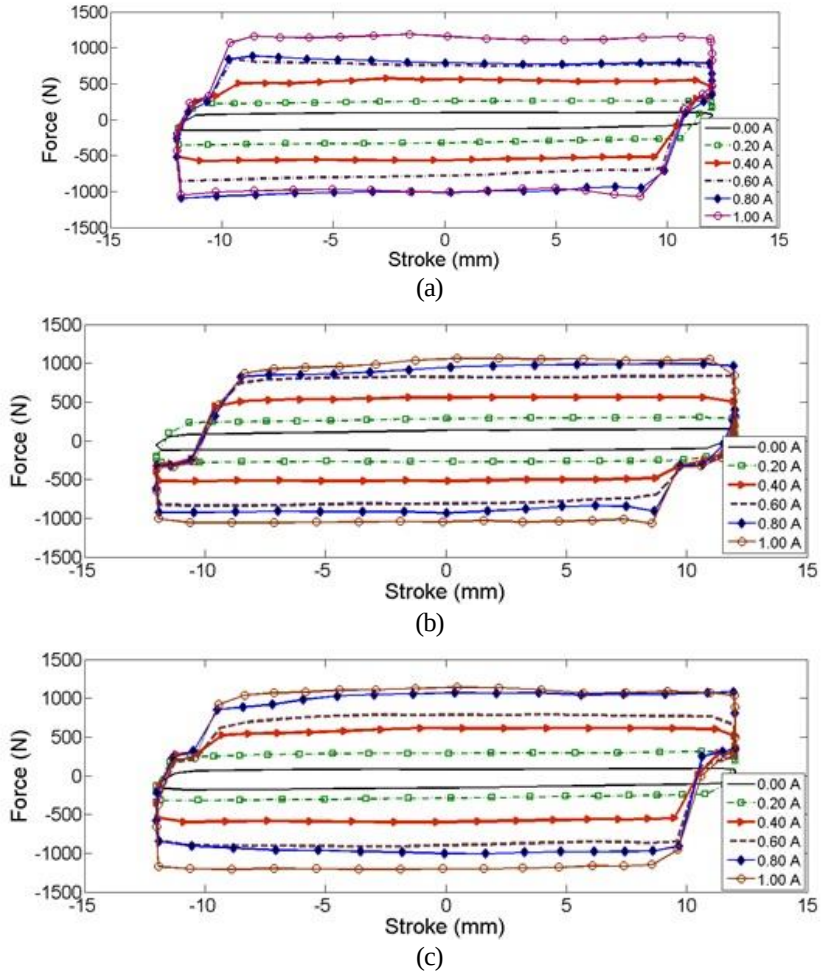

Fig. 9 Force versus stroke length for different current at different stroke positions in cycle mode: (a) first stroke position, (b) mid stroke position and (c) third stroke position

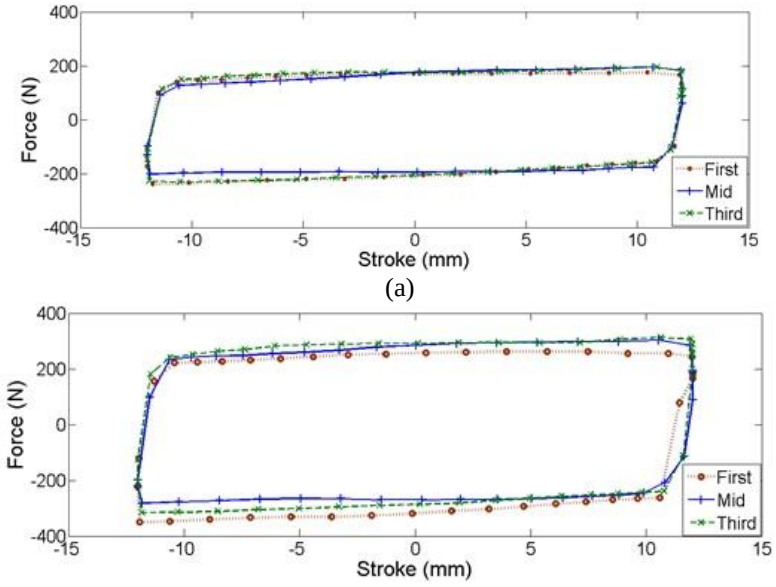

Fig. 10 Comparison of forces at different stroke positions for 12 mm stroke length in cyclic mode: (a) applied current = 0.10 A and (b) applied current = 0.20 A

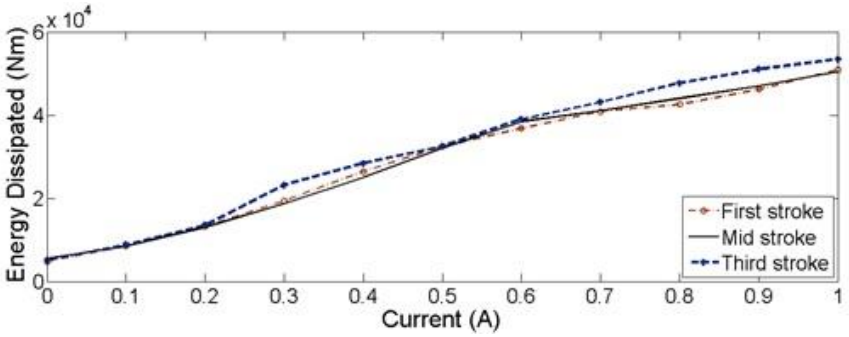

Fig. 11 Energy dissipated in the hysteresis for different current

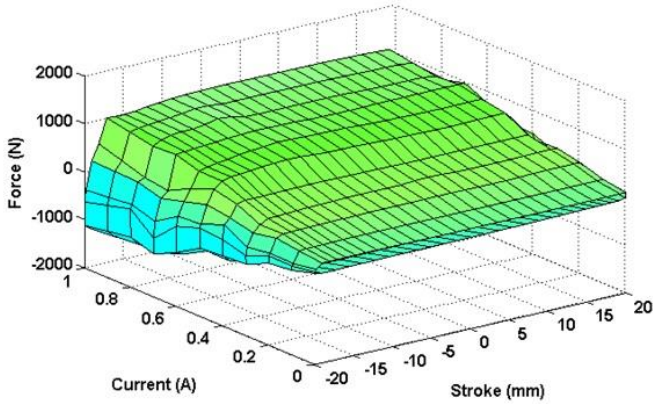

Fig. 12 Three-dimensional plot of current, stroke (or stroke length) and force at mid stroke positions in cycle mode for 20 mm stroke length

Fig. 11 shows the energy dissipation values at varying current. The energy dissipated at different stroke positions are also found to be similar to each other. The slope of this plot changes twice. Slow rise in the beginning turns into a much faster rise in the middle, and after 0.6 A, the slope becomes less steep. The reason behind is similar to that mentioned in the downward motion mode response. Additionally, the chain-like structures of particles tend to be thicker when current is higher which demands a higher force i.e., higher energy dissipation.

Taking the cycle stroke length as 20 mm, the force is plotted against stroke length and current (as in Fig. 12). The piston moves at a constant velocity of 500 mm/min. This data will then be added in the Lookup Table, to be used in the controller development in MATLAB Simulink.

3. Controller development

The amount of damping force produced by an MR damper varies with the external magnetic field. The force response magnitude increases proportionately with increasing field strength. At structure requires more mechanical energy to yield these chain-like structures. In the case of vehicles, the road gives an input excitation to the suspension system of the vehicle the off-state (without field), the force is the smallest as the particles are not attracted to each other. On the other hand, at a higher magnetic field, the alignment of the particles in a rigid chain which might impose discomfort to the users (Fig. 13). Passive damper with constant damping values is not capable of efficiently addressing this issue. Thus, by utilizing an MR damper in the car model, the excitation can be minimized, regardless of the road profile as the amount of damping force can be varied (with varying current).

From Fig. 13, the equations of motion of a quarter car model can be expressed as

$$m_1\ddot{x}_1 + k_1(x_1 - x_2) + d_1(\dot{x}_1 - \dot{x}_2) + f_c = 0 \tag{1}$$

$$\begin{aligned} &m_2\ddot{x}_2 - k_1(x_1 - x_2) - k_2(x_b - x_2) \\ &- d_1(\dot{x}_1 - \dot{x}_2) - d_2(\dot{x}_b - \dot{x}_2) - f_c = 0 \end{aligned} \tag{2}$$

where m_1 is the sprung mass and m_2 is the unsprung mass. d and k are the damping and stiffness elements where subscript 1 represents the suspension and subscript 2 refers to tire-related components. f_c is the damping force provided by the MR damper and x_b is the road surface excitation.

In order to determine the required damping force needed to suppress the vibration, a feedback control system is utilized (Fig. 14).

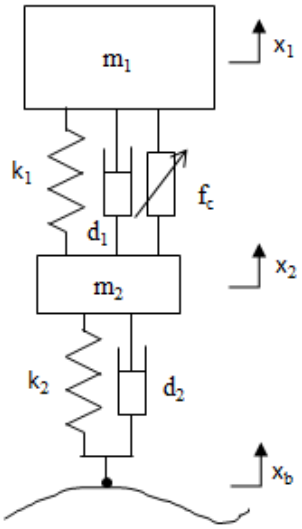

Fig. 13 Quarter car model

In this section, two controllers are being studied and run in MATLAB Simulink, which are PID and F-PID controllers (Fig. 15). The outputs of the system, with and without PID controller were compared for different inputs. Equating m_1=325 kg; m_2=55 kg;d_1=2000 Nsm^{-1}, d_2=250 Nsm^{-1}, k_1=42000 Nm^{-1} and k_2=180000 Nm^{-1}, the results of these simulations are shown in the following subsections.

3.1 PID controller

Assigning the step input as the disturbance to the system, the PID controller's gains are tuned to Kp = 550, Kd = -3000 and Ki = 0. It reduces the settling time to 0.63 second from 1.88 second. The overshoot reduces to 31.5% from 61.3% (Fig. 16(a)). With impulse response as the disturbance, these values of PID controller once again is capable of significantly reduces the disturbance (Fig. 16(b)). Here, the settling time has been reduced to 0.56 second from 1.88 second.

The results in Figs. 16(a) and 16(b) shows that the manually tuned PID controller has worked satisfactorily for both step and impulse inputs. However, it is not that much of efficient in the condition where frequency varies, which is excited with chirp signal input in the simulation (Fig. 17).

Fig. 17 (a) shows the response of chirp signal with PID controller of the same gains. Fig. 17(b) is the sectioned view of Fig. 17(a). Here, it is shown that the response of PID controller is worse than the uncontrolled response. Fig. 17(c) highlights the response 3.5s to 9.8 s to clearly show the output. Thus, to improve the results, a new set of gains is needed. However, manually tuning the gains at every road condition is not viable. Therefore, the implementation of an adaptive controller, which in this work refers to fuzzy rule based PID controller, is designed in MATLAB/Simulink to be implemented in the system.

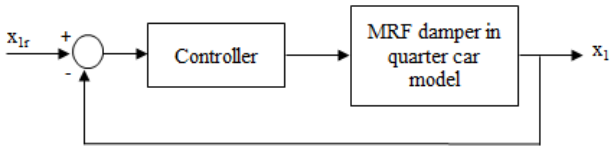

Fig. 14 Block diagram of the feedback control in the quarter car model, utilizing MRF damper

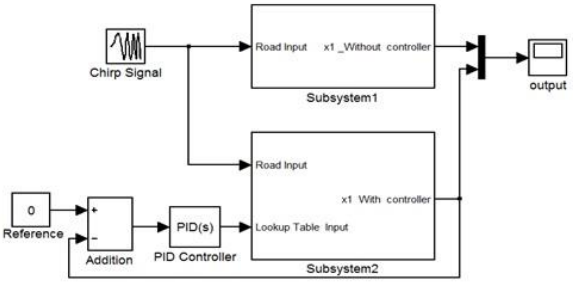

Fig. 15 Simulation of quarter car model in MATLAB Simulink, with PID controller

3.2 Fuzzy based adaptive PID controller

When there is a disturbance from the road, a certain value of magnetic field must be applied to damp the excitation force. Thus, the value of the applied current needed to generate the required amount of magnetic field will be extracted from the Lookup table, which enlisted the values of damping force as well as the associated applied current and piston displacement. The idea of using 'Lookup Table' minimizes the effort of evaluating so many constant parameters, in the derivation of mathematical modelling of the MR damper. Moreover, Lookup table used actual experimental data, which is more practical. Here, the results of the 20 mm cyclic displacement at the mid stroke position (Fig. 12) is considered in the table.

To design a fuzzy-tuned PID controller the triangular membership functions are used for input and output variables as shown in Fig. 19.

The linguistic levels of these inputs and outputs are assigned as N: negative; Z: zero; P: Positive.

Since, the membership function has three variables as input and three variables as output, hence, in the design, it has nine fuzzy rules. The fuzzy PID controller rule base composed of 9 (3x3) rules is shown in Table 3.

The new Fuzzy-PID controller block, modelled in MATLAB/Simulink, is given in Fig. 19.

The uncontrolled and controlled outputs (for both fuzzy-PID and PID controllers) are shown in Fig. 21.

Fig. 21(a) shows the response of PID, fuzzy-PID and uncontrolled responses of the system where as Fig. 21(b) shows the plots from PID and F-PID controlled response. It is observed that the fuzzy-PID controller response is much better than that of PID controller.

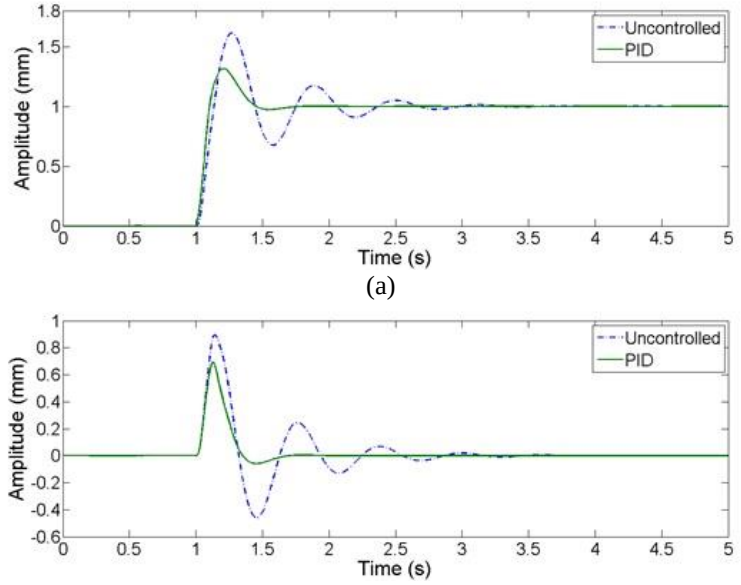

Fig. 16 Results. (a) Step response of PID controller and (b) Impulse response of PID controller

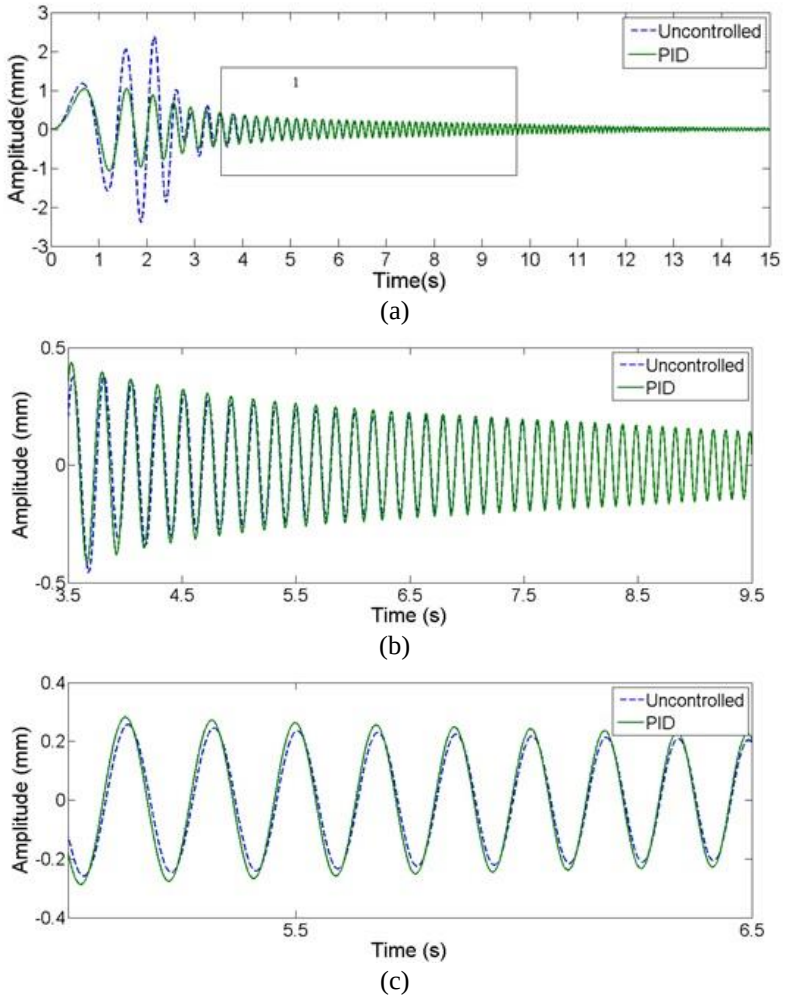

Fig. 17 (a) Chirp signal response of PID controller, (b) Sectioned view of Chirp signal response of PID controller (box marked area-1 in (a)) and (c) zoomed view of view in (b)

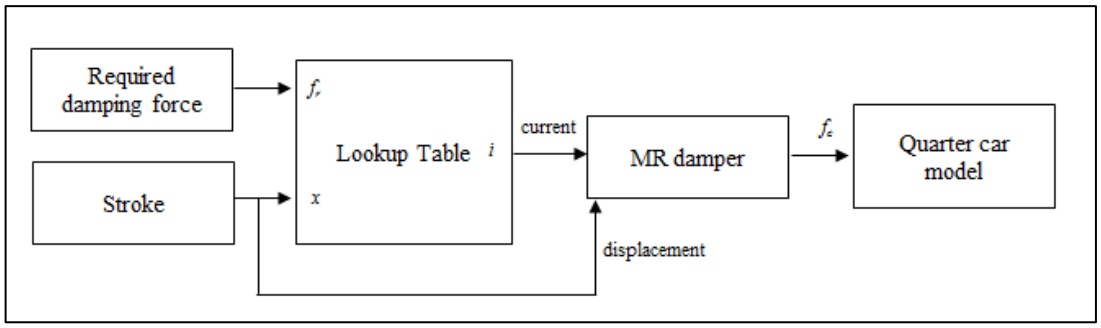

Fig. 18 Block diagram to determine the required value of current to be applied to the MR damper

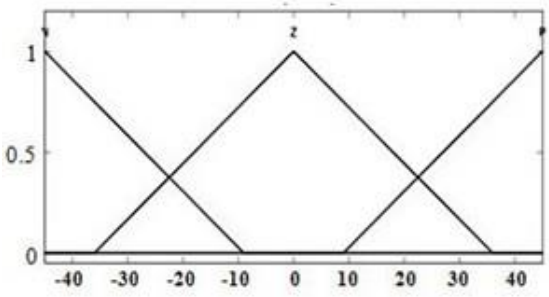

(a) Input variable: error, e(t)

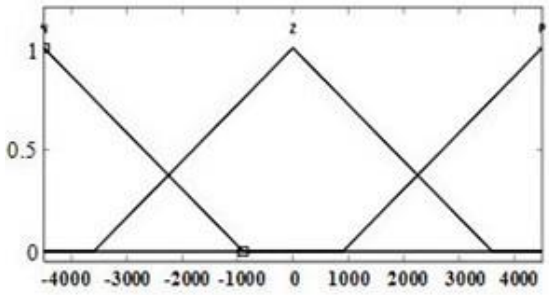

(b) Input Variable: derivative of error, de(t)

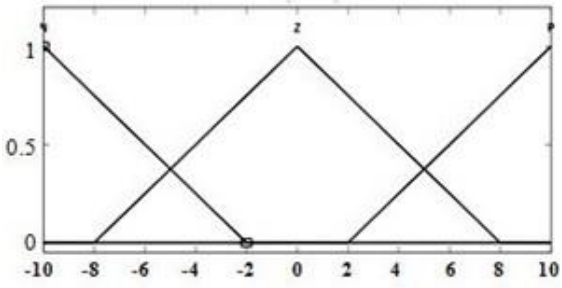

(c) Output variable: Proportional gain, Kp

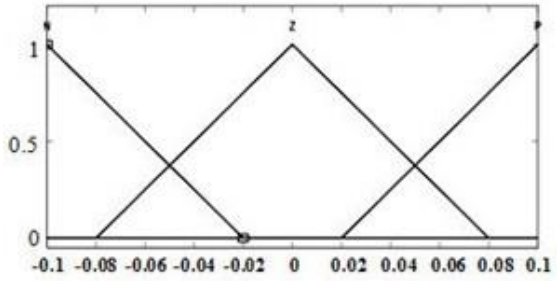

(d) Output variable: Integral gain, Ki

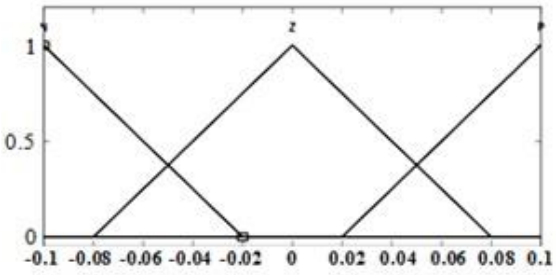

(e) Output variable: Derivative gain, Kd

Fig. 19 Membership functions

On the other hand, Fig. 21(c) focuses on 5.8s < t < 8.8.s, at which in this region, the PID controller does not work efficiently (as explained in Fig 17(c). Again, the fuzzy-PID controller reduces the maximum peak by 68% from that of PID controller in low frequency range. In addition to that, it also reduces the maximum peak by 83% from that of the uncontrolled one. Fuzzy-PID gives better reduction in higher frequency region as well, indicating the superiority of fuzzy-PID controller in a wide range of frequency. Table 4 provides the results of percentage of peak reduction performed by these two controllers.

There are several advantages of the proposed methodology to model the MR damper. Firstly, the characteristic table or the Lookup Table is based on the actual data.

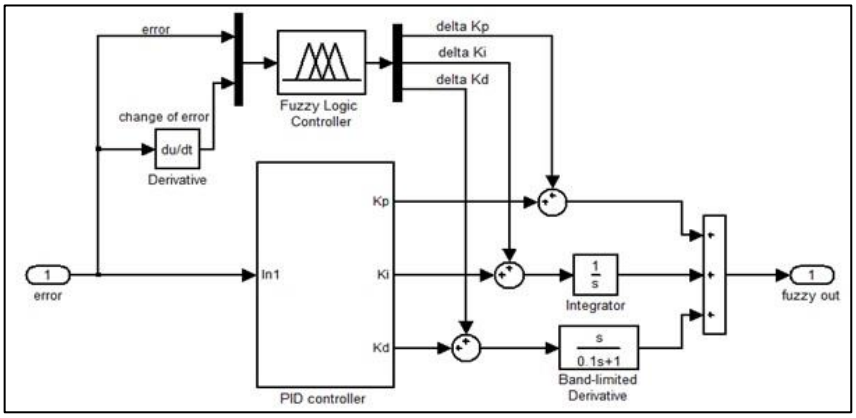

Fig. 20 Simulink model of Fuzzy-PID controller

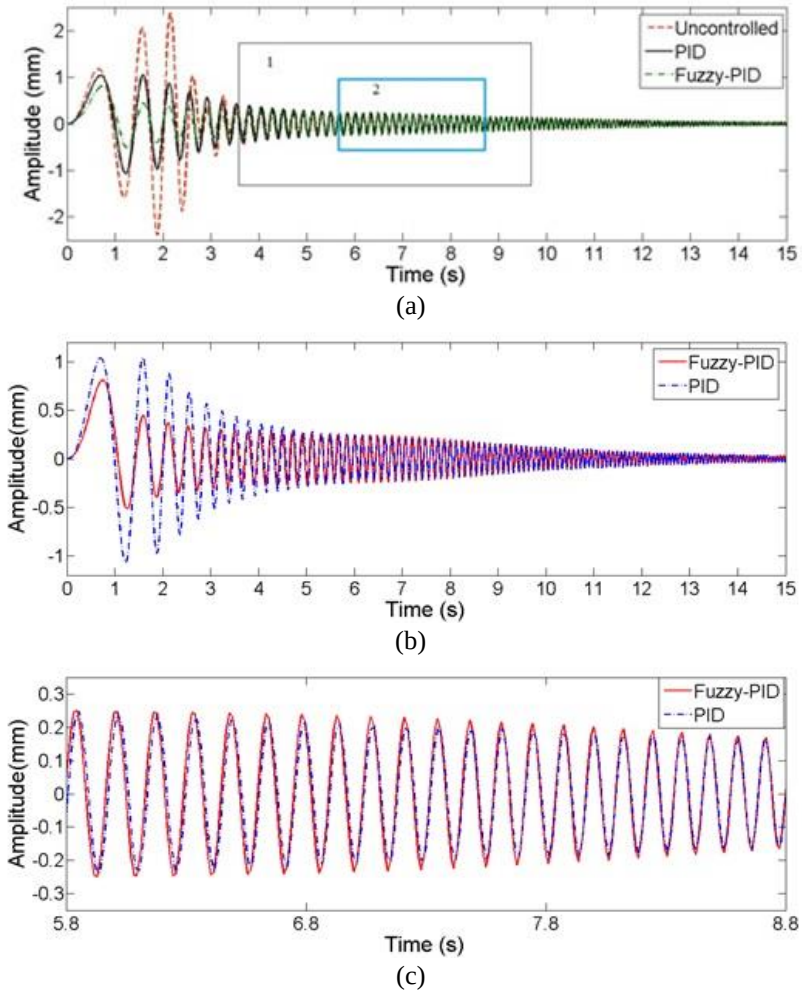

Fig. 21 Controller response for Chirp signal. (a) comparison among uncontrolled, PID and Fuzzy-PID; (b) zoomed view of box-1 marked in (a); (c) zoomed view of box-2 marked in (a)

The MR damper has been tested several times with varying current input and the Lookup Table is designed after taking the average values of force for every current input.

Secondly, only one characteristic table is needed for the damper model. Thirdly, it is simple and acceptable as it is based on the data from the table which allows for a simple controller design. Finally, it minimizes the computational load of many constant parameters. The shortcoming of this model is that in order to get more precise data to accurately

Table 3 Fuzzy PID controller rule base

	e(t)		
de(t)	**N**	**Z**	**P**
N	P	P	Z
Z	P	Z	N
P	Z	N	N

Table 4 Peak reduction: PID controller vs Fuzzy-PID controller

Controller Type	Peak reduction (%)
Uncontrolled response	0
PID controller response	53.2
Fuzzy-PID controller response	83

represent the force-current-displacement analysis, repeated experiments of the same current input to get an average is needed.

4. Conclusions

This paper discusses the advantage of employing Fuzzy-PID controller in magnetorheological (MR) damper, to be implemented in a quarter car model. Experimental investigations and performance analysis were also conducted, which later is used to represent the MR damper dynamics in the controller design. The performance test was based on the dynamic force-displacement (contour) and force-displacement-current (surface) analysis. A lookup table, carrying experimental data, is used to overcome the complexity of dealing with too many parameters estimation in modelling the MR damper. Here, two controllers are studied in order to test the performance of the MR damper in the quarter car model, which are PID and Fuzzy-PID. The results show that in varying frequency conditions, utilizing Fuzzy-PID controller in the system gives better performance with a reduction of 83%, compared with the uncontrolled response.

Acknowledgements

This work was partly supported by Exploratory Research Grant Scheme (ERGS13-020-0053) from the Ministry of Higher Education Malaysia.

References

Antolini, M., Köse, O. and Gurocak, H. (2013), "Haptic device with spherical MR-brake for wrist rehabilitation", *Proceedings of 2013 International Design Engineering Technical Conferences and Computers and Information in Engineering Conference*. Portland, Oregon, August.

Avraam, M.T. (2009), MR-fluid brake design and its application to a portable muscular rehabilitation device, *Doktora Tezi, Université Libre De Bruxelles, Faculté De Sciences Appliquées*.

Babesse, E., Belkhiat, S., Cherif, A., Meddad, M., Eddiai, A. and Boughaleb, Y. (2016), "Improved modal observer for modal SSDI-Max", *Molecular Crystals Liquid Crystals*, **628**(1), 145-161.

Carlson, J.D. and Jolly, M.R. (2000), "MR fluid, foam and elastomer devices", *Mechatronics*, **10**(4), 555-569.

Cha, Y.J. and Agrawal, A.K. (2016), "Robustness studies of sensor faults and noises for semi-active control strategies using large-scale magnetorheological dampers", *J. Vib. Control*, **22**(5), 1228-1243.

Diyana Nordin, N.H., Muthalif, A.G.A., Saleh, T. and Azlan, N.Z. (2015), "Optimal particle ratio to maximize the dynamic range of magnetorheological fluid (MRF) damper for prosthetic limb", *Proceedings of the 10th Asian Control Conference (ASCC)*, Kota Kinabalu, Malaysia, June.

Dong, S., Lu, K.Q., Sun, J.Q. and Rudolph, K. (2006), "Adaptive force regulation of muscle strengthening rehabilitation device with magnetorheological fluids", *Neural Syst. Rehabilit. Eng., IEEE T.*, **14**(1), 55-63.

Ekkachai, K., Tantaworrasilp, A., Nithi-Uthai, S., Tungpimolrut, K. and Nilkhamhang, I. (2014), "Variable walking speed controller of MR damper prosthetic knee using neural network predictive control", *Proceedings of the SICE Annual Conference (SICE)*, Sapporo, Japan, September.

Gordaninejad, F. and Kelso, S.P. (2000), "Fail-safe magneto-rheological fluid dampers for off-highway, high-payload vehicles", *J. Intel. Mat. Syst. Str.*, **11**(5), 395-406.

Hato, M.J., Choi, H.J., Sim, H.H., Park, B.O. and Ray, S.S. (2011), "Magnetic carbonyl iron suspension with organoclay additive and its magnetorheological properties", *Colloid. Surface. A*, **377**(1), 103-109.

Huang, J., Zhang, J., Yang, Y. and Wei, Y. (2002), "Analysis and design of a cylindrical magneto-rheological fluid brake", *J. Mater. Process. Technol.*, **129**(1), 559-562.

Kim, J.H. and Oh, J.H. (2001), "Development of an above knee prosthesis using MR damper and leg simulator", *Proceedings of the IEEE International Conference on Robotics and Automation*, Seoul, Korea.

Kwak, M.K., Lee, J.H., Yang, D.H. and You, W.H. (2014), "Hardware-in-the-loop simulation experiment for semi-active vibration control of lateral vibrations of railway vehicle by magneto-rheological fluid damper", *Vehicle Syst. Dyn.*, **52**(7), 891-908. doi: 10.1080/00423114.2014.906631

Makihara, K., Kuroishi, C. and Fukunaga, H. (2013), "Adaptive multimodal vibration suppression using fuzzy-based control with limited structural data", *Smart Mater. Struct.*, **22**(7), 075031.

Mazlan, S., Ekreem, N.B. and Olabi, A. (2007), "The performance of magnetorheological fluid in squeeze mode", *Smart Mater. Struct.*, **16**(5), 1678.

Najmaei, N., Kermani, M.R. and Patel, R.V. (2015), "Suitability of small-scale magnetorheological fluid-based clutches in haptic interfaces for improved performance", *IEEE/ASME T. Mechatron.*, **20**(4), 1863-1874.

Nakano, H. and Nakano, M. (2014), "Evaluation and training system of muscle strength for leg rehabilitation utilizing an MR fluid active loading machine", *Field and Service Robotics.*

Ekkachai, K., Tantaworrasilp, A., Nithi-Uthai, S., Tungpimolrut, K. and Nilkhamhang, I. (2014), "Variable walking speed controller of MR damper prosthetic knee using neural network predictive control", *Proceedings of the SICE Annual Conference (SICE)*, Sapporo, Japan, September.

Gordaninejad, F. and Kelso, S.P. (2000), "Fail-safe magneto-rheological fluid dampers for off-highway, high-payload vehicles", *J. Intel. Mat. Syst. Str.*, **11**(5), 395-406.

Hato, M.J., Choi, H.J., Sim, H.H., Park, B.O. and Ray, S.S. (2011),

"Magnetic carbonyl iron suspension with organoclay additive and its magnetorheological properties", *Colloid. Surface. A*, **377**(1), 103-109.

Huang, J., Zhang, J., Yang, Y. and Wei, Y. (2002), "Analysis and design of a cylindrical magneto-rheological fluid brake", *J. Mater. Process. Technol*., **129**(1), 559-562.

Kim, J.H. and Oh, J.H. (2001), "Development of an above knee prosthesis using MR damper and leg simulator", *Proceedings of the IEEE International Conference on Robotics and Automation*, Seoul, Korea.

Kwak, M.K., Lee, J.H., Yang, D.H. and You, W.H. (2014), "Hardware-in-the-loop simulation experiment for semi-active vibration control of lateral vibrations of railway vehicle by magneto-rheological fluid damper", *Vehicle Syst. Dyn.*, **52**(7), 891-908. doi: 10.1080/00423114.2014.906631

Makihara, K., Kuroishi, C. and Fukunaga, H. (2013), "Adaptive multimodal vibration suppression using fuzzy-based control with limited structural data", *Smart Mater. Struct*., **22**(7), 075031.

Mazlan, S., Ekreem, N.B. and Olabi, A. (2007), "The performance of magnetorheological fluid in squeeze mode", *Smart Mater. Struct.*, **16**(5), 1678.

Najmaei, N., Kermani, M.R. and Patel, R.V. (2015), "Suitability of small-scale magnetorheological fluid-based clutches in haptic interfaces for improved performance", *IEEE/ASME T. Mechatron*., **20**(4), 1863-1874.

Nakano, H. and Nakano, M. (2014), "Evaluation and training system of muscle strength for leg rehabilitation utilizing an MR fluid active loading machine", *Field and Service Robotics*.

Yin, X., Guo, S., Xiao, N., Tamiya, T., Hirata, H. and Ishihara, H. (2016), "Safety operation consciousness realization of a MR fluids-based novel haptic interface for teleoperated catheter minimally invasive neurosurgery", *IEEE/ASME T. Mechatron.*, **21**(2), 1043-1054.

Zong, L.H., Gong, X.L., Xuan, S.H. and Guo, C.Y. (2013), "Semi-active H∞ control of high-speed railway vehicle suspension with magnetorheological dampers", *Vehicle Syst. Dyn*., **51**(5), 600-626.

CC